SIMULATION OF HIGH RESOLUTION FIELD EMISSION IMAGING IN AN RF PHOTOCATHODE GUN

J. Shao[1], H. Chen, J. Shi, X. Wu, Tsinghua University, Beijing, China
W. Gai, Argonne National Laboratroy, Lemont, IL 60439, USA
C. Jing, S.P. Antipov, Euclid Techlabs LLC, Bolingbrook, IL 60440, USA
F. Wang, SLAC National Accelerator Laboratory, Menlo Park 94025, CA, USA
[1]also at Argonne National Laboratroy, Lemont, IL 60439, USA

Abstract

Precisely locating field emission (FE) emitters on a re-alistic surface in rf structures is technically challenging in general due to the wide emitting phase and the broad energy spread. A method to achieve *in situ* high resolution FE imaging has been proposed by using solenoids and a collimator to select electrons emitted at certain phases. The phase selection criterion and imaging properties have been studied by the beam dynamics code ASTRA. De-tailed results are presented in this paper.

INTRODUCTION

Field emission (a.k.a dark current) is critical in high gradient rf devices. Despite decades of effort the knowledge of its origin on the surface in an rf device is still limited, leading to many questions surrounding this fundamental physical phenomenon [1].

The dynamics of emitted electron depends on its emit-ting phase. Because FE electron can emit during half of the rf period, a blurred pattern of field emitters is usually formed downstream which limits the accurate reproduc-tion of emitters on the surface [2-4].

In this paper, a method to reproduce emitters on the surface with high resolution has been proposed with sole-noids and a collimator. Based on the L-band single-cell photocathode gun at Argonne Wakefield Accelerator facil-ity (AWA), ~100 μm resolution can be obtained with a 0.2 mm diameter aperture on the collimator.

IMAGING PRINCIPLE

The layout of the L-band photocathode gun test stand at AWA is illustrated in Fig. 1(a).
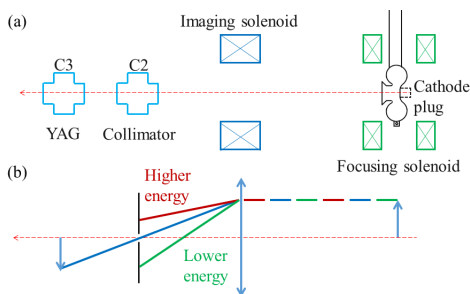

Figure 1: The dark current imaging system at AWA. (a) The beam line layout in simulation: C, vacuum cross; and YAG, doped Yttrium Aluminium Garnet phosphor screen. (b) The equivalent optical imaging system.

Electrons emitted from the cathode gain energy from the gun depending on the emitting phases. They are ac-cordingly focused by the gun and solenoids at different longitudinal positions. The transverse positions of elec-trons depend on their emitting phases and applied focus-ing strength, forming a blurred pattern at the gun exit and deteriorating along the beam line as illustrated in Fig. 2(a-c). When a collimator with a small aperture is applied after the focusing elements, only electrons with the proper focusing position and energy gain are allowed to pass through. A sharp image can be then obtained, as illustrat-ed in Fig. 2(d). The whole imaging system also can be considered as an optical system, as illustrated in Fig. 1(b).
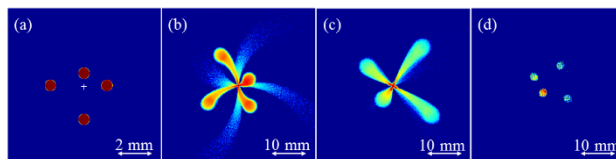

Figure 2: ASTRA simulation results of the emission pat-terns. (a) On the cathode. The white cross indicates the centre of the cathode. (b) At the gun exit. (c) At the imag-ing plane (C3 in Fig. 1) without any collimator. (d) At the imaging plane with a collimator.

MODEL AND PARAMETERS

The beam dynamics has been studied with the code ASTRA [5]. The emitter model used for simulation is illustrated in Fig. 3.
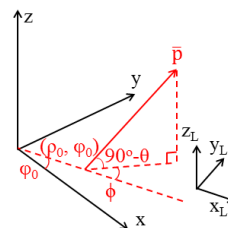

Figure 3: Emitter model in the ASTRA simulation.

The initial emitter position on the cathode is (ρ_0, φ_0) in the polar coordinates. The momentum of the emitted electron is fixed as p, which corresponds to the Fermi energy of copper (7 eV). The emitted current is deter-mined by the emitting rf phase ϑ and emitting angles (θ, ϕ) as illustrated in Fig. 3. The distribution of ϑ can be calculated by the Fowler-Nordheim equation and can be approximated by a Gaussian one. The distribution of ϕ and θ are respectively assumed to be a uniform one from

0 to 2π and a truncated Gaussian one which can be written as

$$f(\theta)=M\exp\left(-\theta^2/(2\sigma_\theta^2)\right) \text{ for } |\theta|\leq\pi/2$$

where σ_θ is standard deviation of θ. The normalized root mean square (RMS) divergence of the emitter α_N can be varied by adjusting σ_θ.

The capture ratio of the system can be defined as

$$\eta=I_{pass}/\int I(\vartheta,\theta,\phi)$$

where I_{pass} is the current that can pass through the aperture. The average magnification and rotation of the imaging system can be defined as

$$\overline{mag}=\bar{\rho}/\rho_0, \quad \overline{rot}=\bar{\varphi}-\varphi_0$$

where (ρ, φ) is the imaging position on the imaging plane. As the system is axial symmetry, the resolution can be defined in radial and angular direction. Assuming ρ and φ follow the Gaussian distribution, the resolutions are defined as

$$R_\rho=2.35\times\sigma_\rho/\overline{mag}, \quad R_\varphi=2.35\times\sigma_\varphi\rho_0$$

where σ_ρ and σ_φ are the standard deviation of ρ and φ. The variations of σ_ρ and σ_φ of adjacent emitters are assumed to be small in the definition.

In simulation, the adjustable parameters of the beam line are the electric filed on the cathode E_c, the focusing solenoid strength B_f, the imaging solenoid strength B_i, and the aperture radius r_{ap}.

PHASE SELECTION CRITERION

At fixed beam line settings, the transverse radius at the aperture of electron emitted at different phases is shown in Fig. 4(a). Electrons from three phase regions can pass through the aperture. Based on their energy gain as illustrated in Fig. 4(b), electrons from the three regions can be defined as the low phase beam, the main beam and the low energy beam, respectively. Because the charge of the main beam is orders of magnitude higher than that of the other two, only the main beam is taken into consideration in the following analysis.
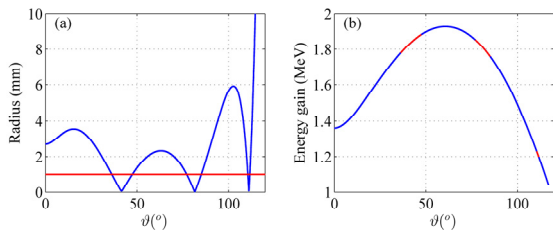

Figure 4: Radius and energy gain at the aperture of electrons emitted at different rf phases. The red line in (a) indicates the aperture radius. The red parts in (b) indicate the emitting phase regions of electrons that can pass through the aperture.

The average emitting phase $\bar{\vartheta}$ of the main beam can be varied by adjusting the beam line parameters. Fix (ρ_0, φ_0)=(1 mm, 0), σ_θ=0, E_c=100 MV/m, B_f=1500 Gauss, and r_{ap}=0.1 mm. The imaging properties with different $\bar{\vartheta}$ are illustrated in Fig. 5. When selecting main beam with higher $\bar{\vartheta}$, the capture ratio and magnification decrease, meanwhile the resolutions improve.
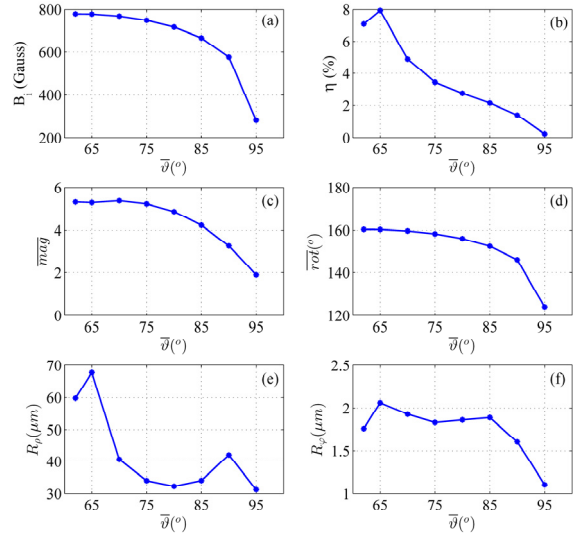

Figure 5: Imaging properties versus $\bar{\vartheta}$.

With the same fixed beam line parameters, the imaging properties of emitters with different ρ_0 are shown in Fig. 6. When $\bar{\vartheta}$ is low and close to the one corresponding to the maximum energy gain, the view range (maximum ρ_0 that can be viewed by the imaging system) on the cathode is limited and the variations of σ_ρ and σ_φ are large. Thus electrons with high $\bar{\vartheta}$ should be selected by the system.
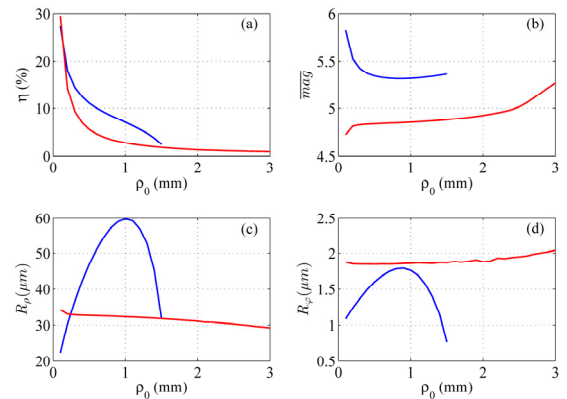

Figure 6: Imaging properties versus ρ_0 for the same fixed beam line parameters as in Fig. 5. The blue and red line indicate $\bar{\vartheta}$=62° and 80°, respectively.

IMAGING PROPERTIES

When $\bar{\vartheta}$ is fixed, the influence of beam line parameters on the imaging properties has also been studied with the ASTRA code.

The Focusing Solenoid Strength B_f

Fix (ρ_0, φ_0)=(1 mm, 0), σ_θ=0, and E_c=100 MV/m. The imaging properties under different B_f is illustrated in Fig. 7. B_i has been adjusted accordingly to select proper $\bar{\vartheta}$. Although higher magnification and better resolution can be achieved with lower B_f, the view range is limited. Thus, high B_f should be applied in the experiment.
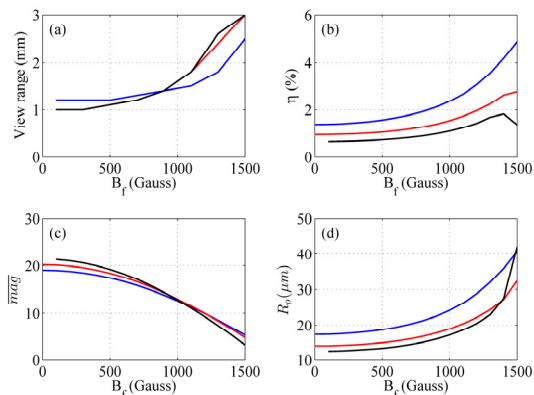

Figure 7: Imaging properties versus B_f. The blue, red, and black line indicates $\bar{\vartheta}$=70°, 80°, and 90°, respectively.

The E-field on the Cathode E_c

Fix (ρ_0, φ_0)=(1 mm, 0), σ_θ=0, and B_f=1500 Gauss. The imaging properties under different E_c is illustrated in Fig. 8. B_i has been adjusted accordingly to select proper $\bar{\vartheta}$. The magnification and resolution improves when high E-field is applied.
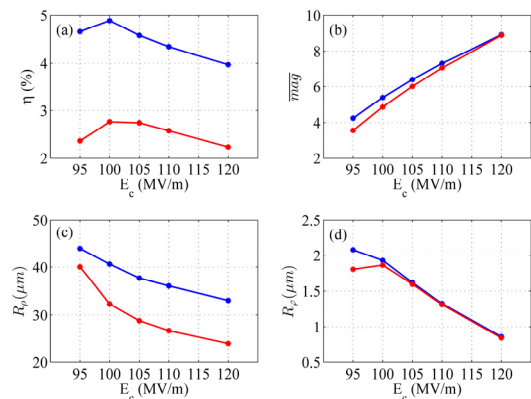

Figure 8: Imaging properties versus E_c. The blue and red line indicates $\bar{\vartheta}$=70° and 80°, respectively.

The Aperture Radius r_{ap}

Fix (ρ_0, φ_0)=(1 mm, 0), B_f=1500 Gauss, and E_c=100 MV/m. The imaging properties under different r_{ap} is illustrated in Fig. 9. The capture ratio, magnification, and rotation remains constant, meanwhile the resolutions deteriorate linearly when increasing r_{ap} for high $\bar{\vartheta}$.

Normalized RMS Divergence α_N

Fix (ρ_0, φ_0)=(1 mm, 0), B_f=1500 Gauss, E_c=100 MV/m, and r_{ap}=0.1 mm. The imaging properties under different α_N is illustrated in Fig. 10. The capture ratio, magnifica-

tion, and rotation remains constant under different α_N. The resolutions can achieve ~100 μm even under the worst case.
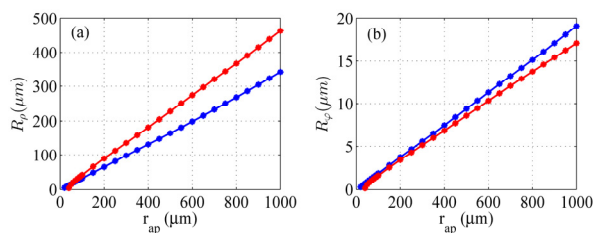

Figure 9: Imaging properties versus r_{ap}. The blue and red, and black line indicates $\bar{\vartheta}$=80° and 90°, respectively.
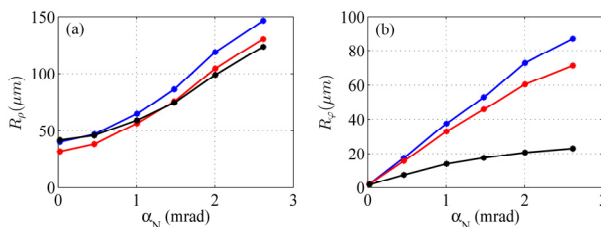

Figure 10: Imaging properties versus α_N. The blue, red, and black line indicates $\bar{\vartheta}$=70°, 80°, and 90°, respectively.

CONCLUSION

A method for *in situ* observation of field emitters with high resolution has been proposed. Electrons from narrow emitting phases have been selected by solenoids and a collimator to form a sharp image. The phase selection criterion and imaging properties have been studied with the code ASTRA. ~100 μm resolution can be achieved with a 0.2 mm diameter aperture.

ACKNOWLEDGEMENT

REFERENCES

[1] arXiv, http://arxiv.org/abs/1604.04086

[2] J.H. Han *et al*., in Proc. PAC'05, pp. 895-897.

[3] A. Moretti *et al*., "Effects of high solenoidal magnetic fields on rf accelerating cavities", Phys. Rev. ST Accel. Beams, vol. 8, p. 072001, 2005

[4] D.H. Dowell *et al*., in Proc. PAC'07, pp. 1299-1301.

[5] *ASTRA-A Space Charge Tracking Algorithm*, DESY, Hamburg, Germany Apr. 2014; http://www.desy.de/~mpyflo/Astra_manual/Astra-Manual_V3.1.pdf.